The Role of Mesoscopic Structuring on the Intermixing of Spin-Polarised Conduction Channels in Thin-Film Ferromagnets for Spintronics

D. Alcer and D. Atkinson

Department of Physics, Durham University, Durham DH1 3LE, United Kingdom

E-mail: david@alcer.de

E-mail: del.atkinson@durham.ac.uk

21 September 2017

Abstract.

The separation of spin-up and spin-down conduction channels is fundamental to electronic transport in ferromagnets and essential for spintronic functionality. The spin states available for conduction are defined by the ferromagnetic material, but additional physical factors can affect scattering and modify the spin-dependence of conduction. Here the effect of mesoscopic structuring, arising during the growth of ferromagnetic thin films, on the electronic transport was investigated. Resistivity and anisotropic magnetoresistance were measured in a series of $Ni_{80}Fe_{20}$ thin films as a function of nominal film thickness from 3 nm up to 20 nm. The observed thickness dependence of the resisivity and magnetic anisotropy of resistivity are intrepreted using a model that accounts for the macroscopic structuring from the growth of the films and incorporates a structural dependence of the spin-flip scattering. The model shows good agreement for both the thickness dependence of the resistivity and the reduction of the anisotropic magnetoresistivity. The latter indicating that increasing mixing of the conducting spin channels occurs in ultra-thin films, mainly a consequence of macroscopic structuring of the films.

Keywords: Spintronics, Anisotropic Magnetoresistance, Film Morphology, Electron-Magnon Scattering, Mott Two-Current Model

1. Introduction

Electronic conduction in ferromagnetic transition metals is understood in terms of the Mott two channel model [1], where spin-up and spin-down electrons propagate in two, largely independent, channels with different resistivities. This conception provides the fundamental underpinning for the functional behaviour exploited in spintronic technologies, such as giant magnetoresistance, that have developed and evolved rapidly in recent decades.

In real ferromagnetic systems, the two spin conduction channels become intermixed to some extent if the spin states of the electrons are not maintained in scattering events. Such spin-flip scattering leads to a loss of the spin-based differentiation of the electronic states exploited in spintronics, which ultimately limits the functional performance of spintronic devices. In many systems such spin-flip scattering results from the interaction of electrons with spin-waves resulting in so-called electron-magnon scattering [2]. Thus for spintronics technology, an understanding and ideally the minimization of spin-flip scattering is important for the design of efficient devices.

Technological needs are driving the performance and scaling of spintronic devices far into the nanoscale regime, both in terms of film thicknesses and the lateral dimensions of structures and devices. For example, the continual increase in hard disk data density requires increasingly high sensitivity magnetoresistive read heads, while a non-volatile magnetic random access memory (MRAM) that is competitive with current semiconductor dynamic random access memory (DRAM) requires minimum feature sizes of the order of ten nanometres. The reduced lengthscale can affect the separation of the spin channels, which reduces device efficiency [3]. A thorough understanding of spin-flip scattering in nanoscale magnetic materials is thus highly topical for spintronics development.

Spin-dependent conduction underpins the physical basis for the observation of anisotropic magnetoresistance (AMR) in ferromagnetic materials [4] [5] and laid the foundations for the later discovery of giant magnetoresistance and the whole field of spintronics [6]. The sensitivity of anisotropic magnetoresistance to two-channel conduction provides a tool for studying and understanding variations of spin-dependent transport, such as the influence of alloying [7, 8, 9] and non-magnetic doping of ferromagnets [5]. However, despite theoretical developments explaining anisotropic magnetoresistance, a fuller understanding of the thickness dependence of AMR for ferromagnetic thin-films with thicknesses on the nanoscale is needed. The sensitivity of AMR to the intermixing of the spin-polarised conduction channels provides a tool to study changes of the spin-dependent conduction within a material, which has relevance to spintronic applications of ultra-thin ferromagnetic films.

Anisotropic magnetoresistance is typically characterized quantitatively by the AMR ratio $\delta\rho/\rho$. In general, the AMR ratio $\delta\rho/\rho$ of sputtered or evaporated ferromagnetic thin-films is significantly lower than that measured in the equivalent bulk ferromagnet, which has been attributed to increased scattering due to an increased density of grain boundaries and impurities [10]. Further, it is commonly observed that the AMR ratio $\delta\rho/\rho$ decreases with decreasing film thickness in the ultrathin regime which was traditionally explained solely by an increase of the resistivity ρ [4], as the resistivity anisotropy $\delta\rho$ was observed to be constant in the thickness range of about $10 - 200\,\mathrm{nm}$ [11], although this result has been questioned [12]. However, more recently a decrease of $\delta\rho$ for ultra-thin films with $t < 10\,\mathrm{nm}$ has been measured by several authors [3, 13, 14].

Building upon the theoretical developments described earlier, Rowan-Robinson *et al.* suggested that the decrease of $\delta\rho$ originates from increased spin-flip scattering associated with reducing film thickness. They implemented a phenomenological thickness dependence for the spin channel intermixing, which scaled approximately with the thickness dependence of the resistivity. This gave good agreement with the experimental data on $\delta\rho/\rho$ [3]. However, while the mechanism of enhancement of electron-magnon scattering was supported by the observation of reduced spin-wave stiffness from temperature dependent magnetisation measurements, this approach cannot provide any quantitative description of the thickness dependence of the resistivity, or model the effective thickness dependence of $\delta\rho$. However, significantly, Rowan-Robinson *et al.* noted that the onset of discontinuities within the structure of the thinnest films is likely to be associated with the reduced spin-wave stiffness.

In this paper the role of film structure on the spin channel intermixing in ferromagnetic thin-films is studied as a function of film thickness, using AMR, to understand the role of mesoscopic film structuring on the spin dependent conduction. Experimental data for thermally evaporated NiFe films are presented as examples of the variations of the resistivity and the AMR as a function of film thickness. A model is developed to describe the magnetotransport, this combines a physical approximation for the thin-film structure emerging from growth, with a structural dependence of the spin-flip scattering. This structural–magnetotransport model gives good agreement with the experimental data.

2. Anisotropic magnetoresistance and spin channel intermixing

Anisotropic magnetoresistance (AMR) describes the resistivity change of ferromagnetic materials upon variation of the relative orientation of the current and magnetization. The AMR-ratio is usually defined as

$$\frac{\delta\rho}{\rho} = \frac{\rho^{\parallel} - \rho^{\perp}}{\rho^{\perp}} \tag{1}$$

where $\delta\rho = \rho^{\parallel} - \rho^{\perp}$ is the resistivity anisotropy [5]. The resistivity in the configuration of a current parallel to the magnetization ($\rho^{\parallel}$) is generally higher than in the perpendicular configuration ($\rho^{\perp}$), leading to a positive resistivity anisotropy and AMR-ratio [4].

Anisotropic magnetoresistance requires spin-dependent conduction [1]. It is based on the different resistivity of the spin-up and spin-down conduction channels [15]. In strong ferromagnets, which are most commonly applied in spintronic devices, the density of d-states at the Fermi energy E_F is strongly spin-split. At E_F the spin-up band structure does not have any d-states into which scattering can occur, and thus this channel has a higher conductivity compared to the spin-down channel which does have d-states at E_F into which spin-down conduction electrons can scatter [7, 8, 9].

Anisotropic magnetoresistance is caused by spin-orbit interaction induced mixing of spin-up and spin-down d-states, as first formulated by Smit [16]. The anisotropy of the scattering rates into the spin-mixed d-states creates an anisotropic contribution to the resistivity [5].

In terms of the Mott two current model, anisotropic magnetoresistance can be described by the equations:

$$\rho = \frac{\rho_{\uparrow}\rho_{\downarrow} + \rho_{\uparrow\downarrow}(\rho_{\uparrow} + \rho_{\downarrow})}{\rho_{\uparrow} + \rho_{\downarrow} + 4\rho_{\uparrow\downarrow}} \tag{2}$$

$$\delta\rho = \gamma\,\frac{(\rho_{\downarrow} - \rho_{\uparrow})\rho_{\downarrow}}{\rho_{\uparrow} + \rho_{\downarrow} + 4\rho_{\uparrow\downarrow}} \tag{3}$$

$$\frac{\delta\rho}{\rho} = \gamma\,\frac{(\rho_{\downarrow} - \rho_{\uparrow})\rho_{\downarrow}}{\rho_{\uparrow}\rho_{\downarrow} + \rho_{\uparrow\downarrow}(\rho_{\uparrow} + \rho_{\downarrow})} \tag{4}$$

which is known as the Campbell-Fert-Jaoul model. $\rho_{\uparrow}$ and $\rho_{\downarrow}$ denote the resistivities of the spin-up and spin-down sub-bands, respectively. $\rho_{\uparrow\downarrow}$ is the spin-flip resistivity, and γ is a constant determined by the relative strength of spin-orbit interaction with respect to the ferromagnetic exchange field [5].

The intermixing of the spin channels, described by the spin-flip resistivity $\rho_{\uparrow\downarrow}$, is due mainly to electron-magnon scattering [17, 7]. As seen from equation (3), it leads to the reduction of the resistivity anisotropy $\delta\rho$. Measurements of $\delta\rho$ can therefore be used as an indicator of changing spin channel intermixing. In contrast, from equation (2), it is clear that there is no strong effect of $\rho_{\uparrow\downarrow}$ on the resistivity ρ, as both the numerator and the denominator increase with increasing $\rho_{\uparrow\downarrow}$. In essence, a strong intermixing equalizes the properties of the spin channels, thus diminishing magnetoresistive phenomena like AMR that originate from the different resistances of the spin-up and spin-down conduction channels.

3. Experimental methods

NiFe alloys with composition around $Ni_{0.8}Fe_{0.2}$ (Permalloy) are well suited to magnetoresistive devices due to the relative large AMR ratio coupled with high permeability and low magnetostriction [10]. Here magnetoresistance in $Ni_{0.8}Fe_{0.2}$ was studied experimentally as a function of nominal film thickness.

NiFe samples were deposited onto cleaned thermally-oxidized Si substrates by high vacuum thermal evaporation. The substrates were maintained at room temperature during deposition. The growth pressure was 5×10^{-7} Torr and the growth rate of 0.4 Å/s. The sample thickness was determined using a quartz crystal thickness monitor that was calibrated using x-ray reflectivity measurements.

Resistivities were measured using a standard in-line 4-probe method. A magnetic field of 50 mT was used for the magnetoresistance measurements, this was much larger than the field required to saturate the samples. The AMR was measured by rotating the plane of the samples through an angular range of 180° in the magnetic field. Surface profiles of the thin-films were measured using an atomic force microscope (AFM) in tapping mode.

4. Experimental results: Film resistivity, magnetoresistance and morphology

The thin film resistivity as a function of thickness is shown in figure 1. Note that the resistivity increases over almost two orders of magnitude. This effect cannot be explained by the established Fuchs-Sondheimer or Mayadas-Shatzkes models, as shown by the modelled lines on the figure 1.

For the AMR, the corresponding resistivity anisotropy is shown in figure 2. $\delta\rho$ is constant for thicknesses down to 10 nm and decreases for thicknesses $t < 10$ nm. For the thinnest sample deposited (nominal $t = 2.9$ nm) a measurement of $\delta\rho$ was impossible due to the very high sample resistivity. Note also that in general the sample-to-sample variations were larger than the electrical measurement errors. From the resistivity and the resistivity anisotropy the AMR ratio is obtained as a function of thickness, see figure 3.

Considering now the film structure, an image of

the surface of a film of thickness $t = 2.9\,\mathrm{nm}$ is shown in figure 4. At this thickness the film structure consists of a series of interconnected islands. This reflects the mode of growth, which includes limited opportunity for surface motion of the arriving adatoms as the substrate is at room temperature.

5. Thickness dependent resistivity and mesoscopic film structure

An increasing resistivity with decreasing film thickness in thin metal films is a long known phenomenon. The explanation in terms of electron scattering at the film boundaries, first suggested by Thomson [18], has attracted much interest. The most significant theoretical formulation was made by Fuchs [19] by solving the Boltzmann transport equation, which was later extended by Sondheimer [20] and, with Sondheimer's convenient approximations, has been widely used to interpret thin-film conductivity data [21, 22, 23, 24]. An interpretation of the resistivity increase incorporating scattering at grain boundaries was formulated by Mayadas and Shatzkes [25, 26]. For polycrystalline films grain boundary scattering commonly dominates over surface scattering, and thus experimental resistivities have often been interpreted in terms of the Mayadas-Shatzkes theory [27, 28, 29, 30, 31, 32].

However, it has been noted that both theoretical models fail to match the sharp increase of resistivity for the thinnest of films [33] and that includes the resistivity data on NiFe films presented here in figure 1.

The dramatic increase in resistivity for the thinnest films is attributed to the growing importance of the mesoscopic film structure and specificially macroscopic surface roughness. When the thickness variation becomes comparable to the sample thickness, the macroscopic surface variations can dominate the electric properties of the sample [34, 35, 36, 33, 37]. In this context, the term *macroscopic surface roughness* is to be understood as roughness on a length scale that is greater than the mean free path of the conduction electrons. For this reason the macroscopic roughness can be treated separately from the microscopic roughness [36]. The influence of *microscopic* roughness can be calculated in a statistical manner using the linear Boltzmann transport equation, as demonstrated by Fuchs [19]. On the other hand, the *macroscopic* roughness can be treated using macroscopic analysis, e.g. by discretization and applying Kirchhoff's first law [36].

The influence of macroscopic surface roughness was modeled in a simplistic manner by Namba assuming a macroscopic sine-wave like surface variation

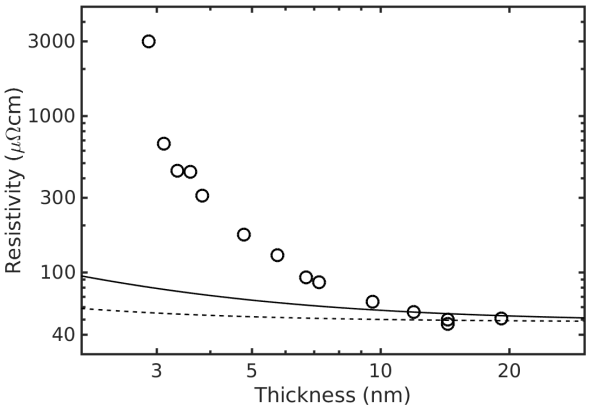

Figure 1: Experimental thickness dependent resistivity ρ of thin NiFe films. The dashed curve represents the Fuchs-Sondheimer model and the solid line the Mayadas-Shatzkes model. For both models a realistic electron mean free path of 1 nm and fully diffuse scattering is assumed. The average grain size in the Mayadas-Shatzkes model is assumed to equal the film thickness.

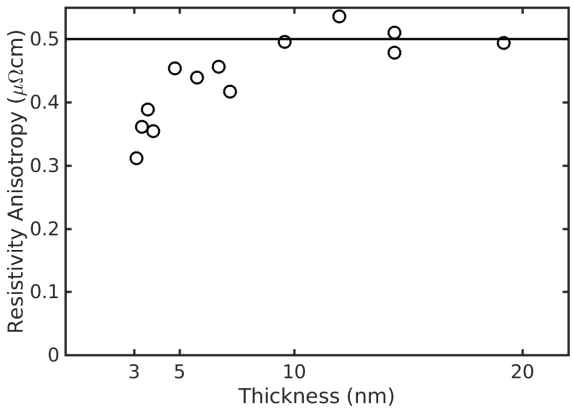

Figure 2: Experimental thickness dependent resistivity anisotropy $\delta\rho$ of thin NiFe films. The solid line illustrates the hypothesis of a constant $\delta\rho$.

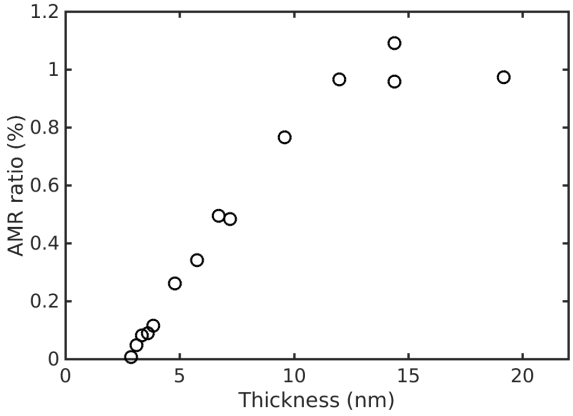

Figure 3: Experimental thickness dependent anisotropic magnetoresistance ratio $\delta\rho/\rho$ of thin NiFe films.

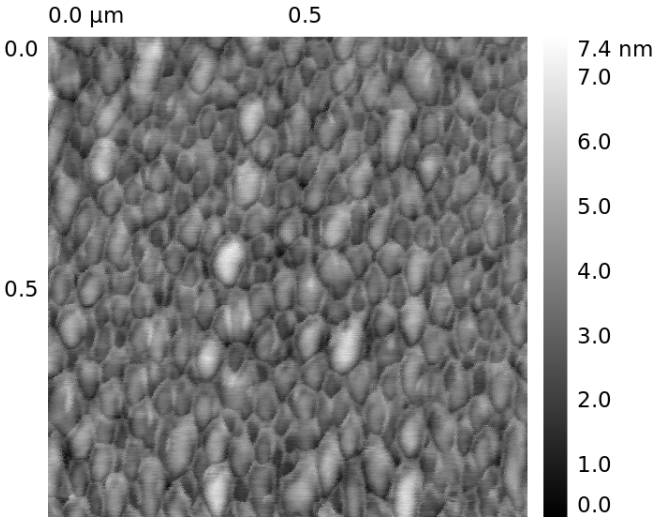

Figure 4: Atomic force microscopy tapping-mode image of a thermally evaporated NiFe film of thickness $t = 2.9\,\mathrm{nm}$.

along the current direction [35]. This approach clearly oversimplifies the film structure, but it has been applied to interpret experimental data by several authors [38, 39]. Elsom *et al.* have pointed out the importance of a realistic model of the surface structure to account for the more complicated thickness dependent conduction behavior of real films, including percolation effects. They developed a conduction model, based on a very simple model for the sample structure, which showed good agreement with resistivity data for several materials [36].

6. A phenomenological model for the macroscopic structure of thin-films

In order to investigate the influence of macroscopic roughness on spin-channel intermixing, a model for the film structure that reproduces the main features of thin film structure is needed. Atomic scale models are capable of describing the growth process in great detail, however, typically a large number of parameters are needed for a good representation of the film morphology [40, 41, 42, 43] and such a detailed description of the growth process is not justified when only the main macroscopic features of the films need to be represented. Thus a much simpler model can be developed.

Here the surface structure simulation methodology is based on the Elsom model [36], where the morphology is modelled with a random distribution of individual islands. Each island is approximated as a truncated cone of base diameter, D, and a fixed thickness, H. For the simulation of film structure a number of these islands are placed in random locations. The number of the islands depend on the film thickness. When the simulated structure 'grows' the cones overlap and form a continuous film.

This very simple structural model represents the real sample structure of thin films fairly well. The only substantial discrepancy between model and reality lies in a difference in contrast between the highest and lowest features. In the simulation, the tallest accumulations of islands are substantially more pronounced. Also, it is noted that even for thicker films voids are present in the simulations. In these uncovered areas of the sample, no deposition has occurred during the simulation. Both of these features are observed to a reduced extent in real films, due to the migration of surface atoms. On average, such surface atom migration is likely to reduce the tallest features and fill the voids, leading to a somewhat smoother surface. To address these deficiencies of the simple model, two new extensions to the Elsom model have been implemented:

- Growth of individual islands. Each island is modeled to grow to double its original size after it has been deposited. The time scale at which the growth takes place corresponds to a deposited thickness of about $3 - 4\,\mathrm{nm}$.
- Reduced probability of deposition on top of an existing island. While a new island will be randomly located on an empty substrate, deposition on top of previously added island can take place but with a reduced probability, chosen to be $p = 10\,\%$. In the case of no deposition, a new random location is chosen and the concerned time step is repeated.

The addition of these rules remedies the discrepancy between the real and simulated films regarding the extent of the highest and lowest features. While the growth of individual islands is a reasonable assumption for real films, the reduced probability of deposition on top of an island is clearly an artificial addition with little direct physical meaning. However, it may be considered as an equivalent of reduced surface migration onto pronounced structures and/or enhanced migration into voids. The addition of this rule has a similar effect to surface migration in a real film. But most importantly it provides a simple rule set to create more realistic macroscopic structures.

The parameters needed in the model were obtained from fitting to the experimentally observed structural data from AFM measurements. The cone base diameter (D) distribution was modelled as a Gaussian fitted to the experimental island size distribution, as shown in figure 5. While the profile of the individual islands was matched to the measured island shape, as shown in the inset of figure 5. With these parameters the extended model was used to simulate

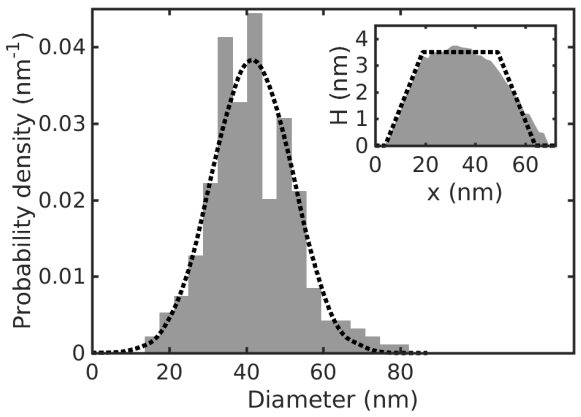

Figure 5: Histogram of the base diameter distribution of the islands at $t = 2.9\,\text{nm}$, taken from atomic force microscopy. The dotted curve shows the base diameter distribution used in the model at the same growth stage. Inset: Measured line profile of an island as a gray area. The dotted line represents the simulated island profile.

thin-film structures.

For example, a simulation of a nominal 3 nm thick film is shown in the top panel of figure 6 and compared with an AFM scan of the surface structure of a 3 nm NiFe thin-film. First, note for such ultra-thin films (e.g. $t = 3.0\,\text{nm}$) that the macroscopic surface roughness is comparable to the average sample thickness.The comparison shows that the macroscale features are comparable, while the high spatial resolution of the AFM also shows some microscale topological features in the real film. Thus, with the additions to the Elsom model, the structural modelling here provides a good representation of the mesoscopic structure of the real films.

7. Modelling the macroscopic structure dependence of resistivity and AMR

From figure 6 it is clear that for very small thicknesses the films show strong nanostructuring, which becomes less significant for thicker films. Such strong structuring in ultra-thin films may be expected to resemble assemblages of interconnected nanoparticles, while thicker films approach the bulk material behavior. This macroscopic structuring will have a direct effect upon the effective resistivity, as a continuous conductive sheet becomes a network of conductive pathways as the thickness decreases.

More signficantly, it is recognized that both magnetic nanoparticles and nanowires can exhibit a

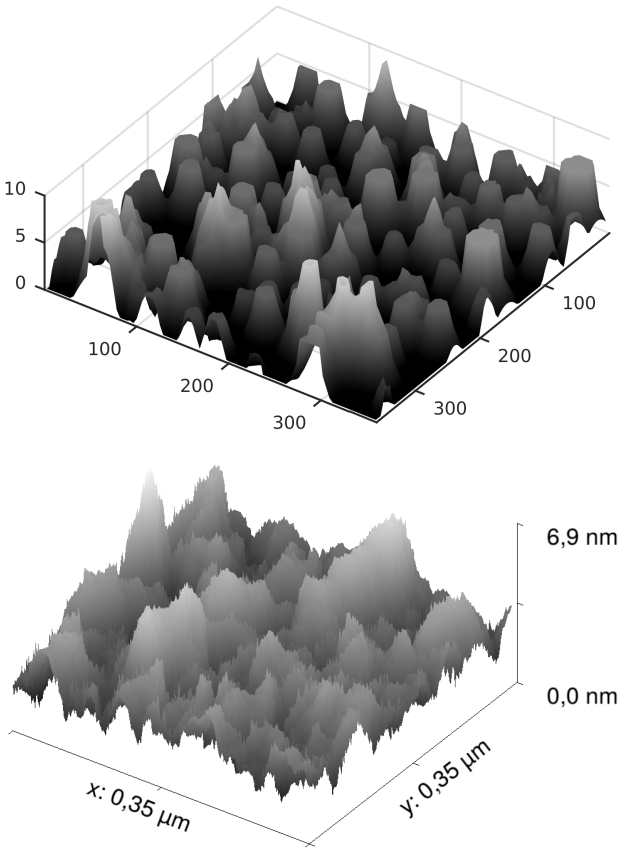

Figure 6: Upper, simulated surface structure of a simulated structure with thickness $t = 3.0\,\text{nm}$. Lower, atomic force microscopy surface image measured on a 3 nm NiFe film. All dimensions are given in nm.

significantly reduced saturation magnetization [44, 45, 46, 47, 48]. This effect is usually associated with strong magnetic disorder and spin-glass like behaviour at the nanoparticle surface [49, 50, 51, 52]. Such magnetic disorder lead to an increase in the magnon density of states, which has often been measured indirectly through the magnetization temperature dependence [45, 46, 47].

Thus increased disorder arising from the macroscopic structuring that occurs in ultrathin films will increase the density of magnon states. Within such nanostructured networks, the smallest scale features will produce local increases of the magnon density of states, which will enhance the spin-flip scattering and hence increase the mixing of the spin conduction channels. This will affect all spin-dependent magnetotransport effects. This will result in a local reduction of the anisotropic magnetoresistance.

A further increase in electron-magnon induced spin-flip scattering is also expected from the electronic confinement in extremely thin films [53]. However this

effect only becomes significant in films with thickness below $t < 2nm$.

Here the effects of the film structure and the associated magnetic disorder of a film have been incorporated into a model to describe the resistivity and anisotropic magnetoresistance of thin-films with mesoscopic structuring. This electrical transport model uses the modelled film structures described in section 6 and assigns a local AMR ratio that depends upon the effective cluster size. For regions above a certain size, the bulk AMR ratio is assumed, while for decreasing cluster size the local AMR ratio decreases. The critical cluster size was used as a fit parameter.
The electrical current flow through the simulated structures was calculated in order understand the effect of the macroscopic surface roughness. It has to be noted that the length scale of the simulated sample roughness (i.e. the island size) is well above the bulk electron mean free path. In addition to the macroscopic roughness, a microscopic roughness also leads to Fuchs-Sondheimer-type scattering. A value for the bulk electron mean free path of $\lambda = 1\,\mathrm{nm}$ was calculated by extrapolation from the resistivity the $\lambda \cdot \rho$ data in ref. [54]. To obtain the local conductivity, total diffuse scattering within the Fuchs-Sondheimer model was assumed, which is a good approximation in most cases [55].

In order to calculate the sample resistivity, a square grid of resistors connected at the adjacent voltage nodes was defined. The resistance of the resistor was obtained from the value of the local resistivity, which was calculated with the Fuchs-Sondheimer model using the local thickness from the structural simulation. The nodes at two opposite edges of the sample form the conductive contacts and according boundary conditions are applied. When Ohm's law is applied to each resistor and Kirchhoff's rule to each node, a (sparse) linear system of equations with $3n^2$, where n is the grid size, variables and equations is found. $n = 100$ was used throughout this work. A relaxation method was used to solve the system and find the current flow through each resistor. The resistance of the sample was found simply from the applied voltage and the overall current flowing between the contacts. Knowing the lateral dimensions, the average sample thickness was used to calculate the resistivity from the resistance. Large-scale ensemble testing with over 1000 simulated film structures for each thickness was used to account for statistical variations.

8. Magnetotransport simulation results

The electrical transport model developed was used to simulate the magnetoresistive response of NiFe thin-films as a function of film thickness. Figure 7 shows examples of the simulations of the structure, AMR ratio and the distribution of electrical power dissipation for 3 nm and 8.5 nm thin-films. The structural simulations, figure 7(a) 3 nm and 8.5 nm (b), show the mesoscopic structuring resulting from island growth and the presence of voids in the thinner film.

Figure 7(c) and (d) show the simulated distributions of the AMR ratio values in the 3 nm and 8.5 nm films respectively. The AMR values are assigned in the model according to the reasoning and methodology described in section 7. In essence, the AMR ratio reduces as a function of size for smaller structural clusters because of increased spin-mixing due to enhanced electron-magnon scattering that is the result of increased magnon density in magnetic nanostructures. It is clear that the AMR ratio is lower than the bulk value and highly variable across the 3 nm film compared to the 8.5 nm thick film.

The anisotropic magnetoresistance response of a film depends upon the AMR ratio distribution and, critically, upon the pathways of current flow. The overall resistance is determined by the resistive pathways through films and a good measure for the local contribution to the overall resistance is the locally dissipated power density. The local power dissipation is shown in figure 7 (e) and (f). The conduction is very inhomogeneous for the thinnest films, like a percolative network, where almost all the power dissipation occurs at a few bottlenecks of conduction. These bottlenecks of conduction are typically thin, poorly conductive parts of the sample. As the overall sample resistivity is mainly determined by the bottlenecks, it is strongly enhanced in the very thin films. This resistivity increase mainly originates from the macroscopic surface structuring. The inhomogeneity of conduction diminishes for thicker films as the film develops into a continuous layer, thus the relevance of the macroscopic surface roughness decreases and the film resistivity approaches the bulk value.

Returning to the magnetoresistive response of a film, this is determined by the current flow and the AMR ratio along the current pathway. The main mechanism for increased spin channel intermixing for ultra-thin films becomes clear from a comparison of the power dissipation shown in figure 7 (e) and (f) with the local AMR ratio in figure 7 (c) and (d). The resistivity of the sample is mainly determined by the conduction bottlenecks, which are typically not part of the larger cluster structures. Rather they form the most nanostructured part of the sample. By their nature these nanoscopic conduction bottlenecks are

more highly magnetically disordered and so have low local AMR ratio. Therefore, the magnetoresistance of the whole sample, dominated by the bottleneck regions, will be reduced. An increased spin-channel intermixing is thus expected for ultra-thin samples as soon as the nanostructuring due to macroscopic roughness dominates the morphology.

9. Comparison between Simulations and Experiment

The structural-electrical transport model was used to simulate the effective resistivity and the anisotropic magnetoresistance as a function of film thickness for comparison with experimental results from NiFe thin-films. The symbols in figure 8 show the measured electrical resistivity of NiFe films as a function of nominal film thickness. The error bars on the film thickness are estimated from the x-ray reflectivity calibration of the deposition rate monitor. The solid line in figure 8 shows the simulated resistivity as a function of film thickness. The simulated resistivity agrees well with the measured results. This analysis shows that almost all of the increase in the resistivity for the thin films is due to the geometrical effects of the mesoscopic structuring, while only $1-5\,\%$ of the resistivity increase is attributed to the microscopic surface roughness described by the Fuchs-Sondheimer model.

A comparison of the experimental and modelled thickness dependence of the magnetic resistivity anisotropy, using the same model parameters as in figure 8, is shown in figure 9. The solid line again represents the simulated thickness dependence, which reproduces the characteristic fall in the experimental resistivity anisotropy for thicknesses below $t = 10\,\mathrm{nm}$. This thickness may be viewed as the onset of a transition from a coherently structured film to a more strongly nanostructured and thus magnetically disordered system. The origin of this transition lies in the macroscopic surface structuring, which dominates the structure of the thinner films. The magnetic disordering leads to enhanced spin-channel intermixing, which in turn decreases the magnitude of magnetoresistive effects. To comprehend any changes in the AMR it is most helpful to study the dependence of the resistivity anisotropy $\delta\rho$, however, for applications the AMR ratio is the most commonly quoted parameter. Here the experimentally derived AMR ratio is compared with the model, see figure 10. Again the agreement is good and the results show that the effective AMR ratio falls to zero as a function of nominal film thickness.

Finally, other mechanisms for the enhanced magnetic disorder were also investigated. These include a simple thickness-dependent ansatz, where the local AMR ratio was assumed to be dependent of the thickness. Agreement with the experimental data could not be achieved with such a model. This confirms, that not the decreased thickness in itself, but the nanostructuring of the thin films leads to the increased spin-channel intermixing.

10. Conclusion

It has been shown that mesoscale surface structuring in ferromagnetic thin-films can lead to a reduction of AMR for thinner films. The mechanism for this reduction is due to spin channel intermixing which increases in thinner films due to an increase in electron-magnon scattering, which is linked to an enhancement of the magnon-density in the thinner, more structurally and magnetically disordered films.

A simple but realistic model for the film structure was presented. Most of the necessary parameters for the model could be obtained from structural investigation of the evaporated films. Using this model for the film structure we have calculated the thickness dependent film resistivity and magnetoresistance anisotropy, both in good agreement with experimental results for thermal evaporated NiFe films. We have shown that the resistivity and the spin-flip scattering are both dominated by the mesoscopic structuring of thin films.

This is a significant result towards the goal to fabricate highly efficient spintronic devices based on reduced spin channel intermixing.

Acknowledgments

We are grateful for the scholarship provided to D. Alcer by the Erasmus+ program. We thank Dr. M. Cooke (School of Engineering and Computing Sciences, Durham University) for assistance with the AFM measurements.

References

[1] Nevill Francis Mott. The electrical conductivity of transition metals. In *Proceedings of the Royal Society of London A: Mathematical, Physical and Engineering Sciences*, volume 153, pages 699–717. The Royal Society, 1936.

[2] Igor Žutić, Jaroslav Fabian, and S Das Sarma. Spintronics: Fundamentals and applications. *Reviews of modern physics*, 76(2):323, 2004.

[3] RM Rowan-Robinson, AT Hindmarch, and D Atkinson. Enhanced electron-magnon scattering in ferromagnetic thin films and the breakdown of the mott two-current model. *Physical Review B*, 90(10):104401, 2014.

[4] T McGuire and RL Potter. Anisotropic magnetoresistance in ferromagnetic 3d alloys. *IEEE Transactions on Magnetics*, 11(4):1018–1038, 1975.

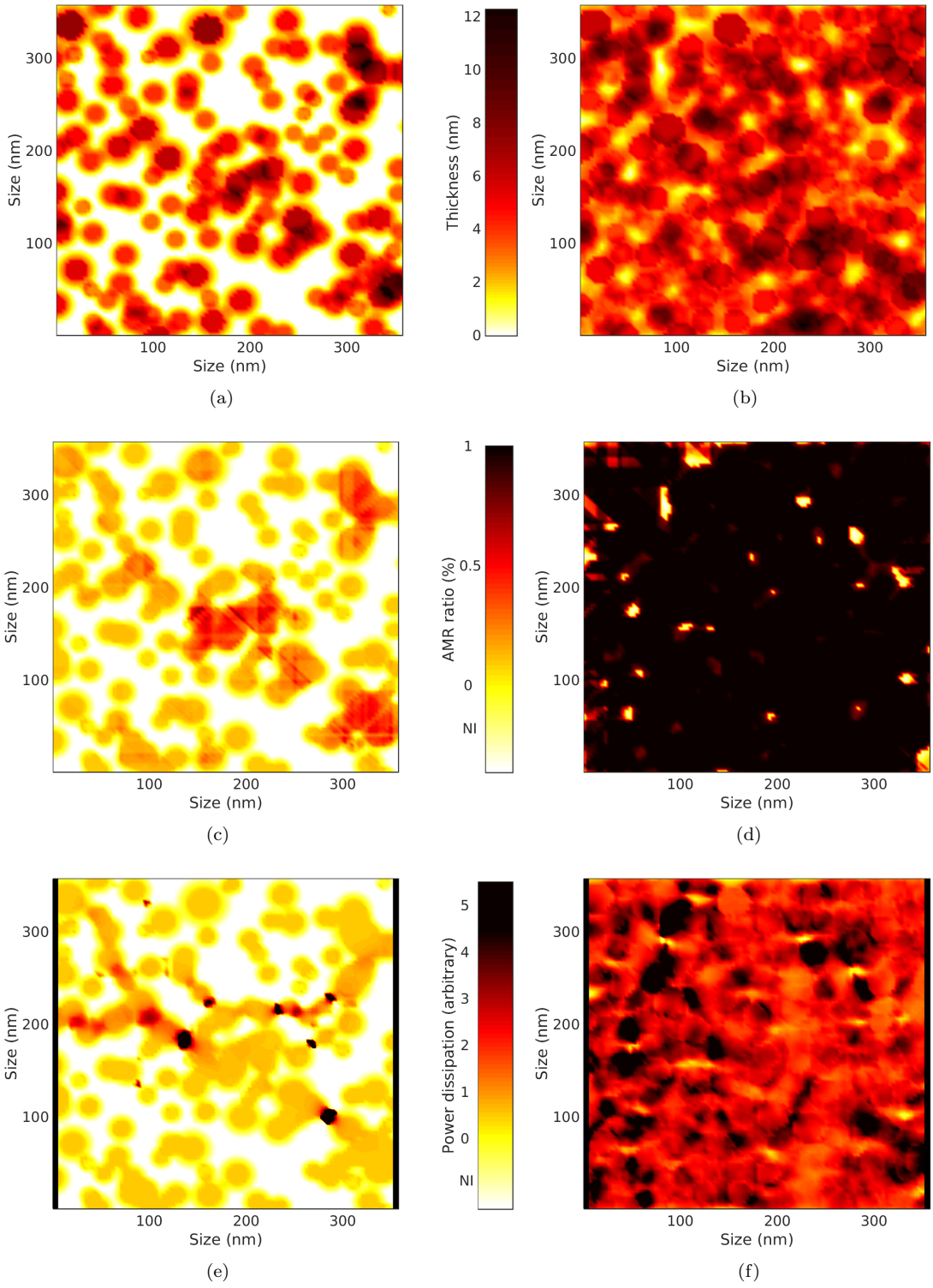

Figure 7: (Colour on-line) Simulation results for two samples. The sample thickness is $t = 3.0\,\mathrm{nm}$ for the sample on the left [(a), (c) and (e)] and $t = 8.5\,\mathrm{nm}$ on the right side [(b), (d) and (f)]. (a) and (b) Sample structure of simulated films. The color scale is not linear for thin parts of the sample to become visible. (c) and (d) Local anisotropic magnetoresistance ratio of simulated films. Dark areas show an AMR ratio approaching the bulk value, while the local AMR ratio in lighter parts is reduced due to magnetic disorder. On the color bar, 'NI' corresponds to areas where no island is present. (e) and (f) Simulated local power dissipation. The voltage is applied between the contacts (designated by thin black bars) on the left and right sides of the sample. On the color bar, 'NI' corresponds to areas where no island is present.

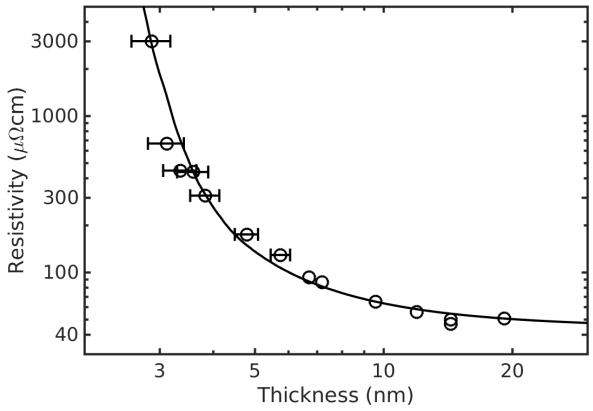

Figure 8: Experimental thickness dependent resistivity ρ of thin NiFe films. The solid curve corresponds to a best fit with the model introduced in section 6. The sample-to-sample variations are bigger than the electrical measurement errors.

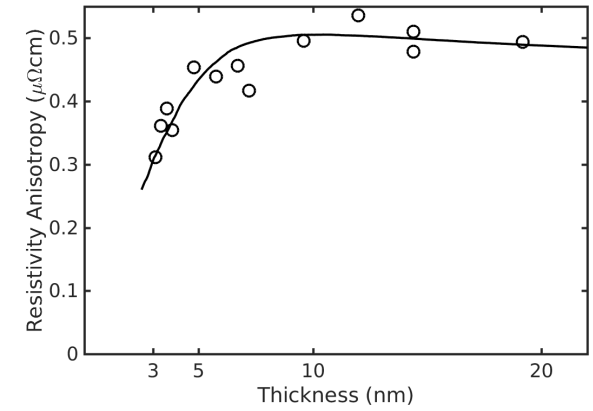

Figure 9: Experimental thickness dependent resistivity anisotropy $\delta\rho$ of thin NiFe films. The solid curve corresponds to a best fit with the model introduced in sections 6 and 7. The sample-to-sample variations are bigger than the electrical measurement errors.

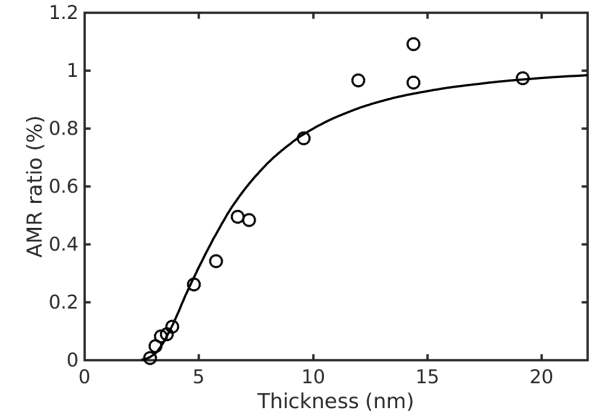

Figure 10: Experimental thickness dependent anisotropic magnetoresistance ratio $\delta\rho/\rho$ of thin NiFe films. The solid curve corresponds to a best fit with the model introduced in sections 6 and 7. The sample-to-sample variations are bigger than the electrical measurement errors.

[5] IA Campbell, A Fert, and O Jaoul. The spontaneous resistivity anisotropy in ni-based alloys. *Journal of Physics C: Solid State Physics*, 3(1S):S95, 1970.

[6] Albert Fert. Nobel lecture: Origin, development, and future of spintronics. *Reviews of Modern Physics*, 80(4):1517, 2008.

[7] A Fert and IA Campbell. Electrical resistivity of ferromagnetic nickel and iron based alloys. *Journal of Physics F: Metal Physics*, 6(5):849, 1976.

[8] O Jaoul, IA Campbell, and A Fert. Spontaneous resistivity anisotropy in ni alloys. *Journal of Magnetism and Magnetic Materials*, 5(1):23–34, 1977.

[9] AP Malozemoff. Anisotropic magnetoresistance of amorphous and concentrated polycrystalline iron alloys. *Physical Review B*, 32(9):6080, 1985.

[10] Th GSM Rijks, R Coehoorn, MJM De Jong, and WJM De Jonge. Semiclassical calculations of the anisotropic magnetoresistance of nife-based thin films, wires, and multilayers. *Physical Review B*, 51(1):283, 1995.

[11] EN Mitchell, HB Haukaas, HD Bale, and JB Streeper. Compositional and thickness dependence of the ferromagnetic anisotropy in resistance of iron-nickel films. *Journal of Applied Physics*, 35(9):2604–2608, 1964.

[12] Frederick C Williams Jr and EN Mitchell. A study of resistance and magnetoresistance in nickel-iron thin films. *Japanese Journal of Applied Physics*, 7(7):739, 1968.

[13] NT Thanh, LT Tu, ND Ha, CO Kim, CheolGi Kim, KH Shin, and B Parvatheeswara Rao. Thickness dependence of parallel and perpendicular anisotropic resistivity in ta/nife/irmn/ta multilayer studied by anisotropic magnetoresistance and planar hall effect. *Journal of Applied Physics*, 101(5):053702, 2007.

[14] Lara Bogart. *An investigation of the structure, pinning and magnetoresistance of domain walls in $Ni_{81}Fe_{19}$ planar nanowires*. PhD thesis, Durham University, 2010.

[15] IA Campbell and A Fert. Transport properties of ferromagnets. *Handbook of Ferromagnetic Materials*, 3:747–804, 1982.

[16] J Smit. Magnetoresistance of ferromagnetic metals and alloys at low temperatures. *Physica*, 17(6):612–627, 1951.

[17] A Fert. Two-current conduction in ferromagnetic metals and spin wave-electron collisions. *Journal of Physics C: Solid State Physics*, 2(10):1784, 1969.

[18] JJ Thomson. On the theory of electric conduction through thin metallic films. In *Proc. Cambridge Philos. Soc*, volume 11, pages 120–123, 1901.

[19] K Fuchs. The conductivity of thin metallic films according to the electron theory of metals. In *Mathematical Proceedings of the Cambridge Philosophical Society*, volume 34, pages 100–108. Cambridge Univ Press, 1938.

[20] E Hi Sondheimer. The mean free path of electrons in metals. *Advances in physics*, 1(1):1–42, 1952.

[21] EC Crittenden Jr and RW Hoffman. Thin films of ferromagnetic materials. *Reviews of Modern Physics*, 25(1):310, 1953.

[22] VVR Narasimha Rao, S Mohan, and P Jayarama Reddy. Electrical resistivity, tcr and thermoelectric power of annealed thin copper films. *Journal of Physics D: Applied Physics*, 9(1):89, 1976.

[23] D Schumacher. New evidence for the validity of the fuchs-sondheimer theory. *Thin Solid Films*, 152(3):499–510, 1987.

[24] L Krusin-Elbaum and MO Aboelfotoh. Unusually low resistivity of copper germanide thin films formed at low temperatures. *Applied physics letters*, 58(12):1341–1343, 1991.

[25] AF Mayadas, M Shatzkes, and JF Janak. Electrical resistivity model for polycrystalline films: the case of

specular reflection at external surfaces. *Applied Physics Letters*, 14(11):345–347, 1969.

[26] AF Mayadas and M Shatzkes. Electrical-resistivity model for polycrystalline films: the case of arbitrary reflection at external surfaces. *Physical review B*, 1(4):1382, 1970.

[27] MA Angadi and LA Udachan. Electrical properties of thin nickel films. *Thin Solid Films*, 79(2):149–153, 1981.

[28] JWC De Vries. Temperature and thickness dependence of the resistivity of thin polycrystalline aluminium, cobalt, nickel, palladium, silver and gold films. *Thin Solid Films*, 167(1-2):25–32, 1988.

[29] N Artunç and ZZ Ozturk. Influence of grain-boundary and surface scattering on the electrical resistivity of single-layered thin copper films. *Journal of Physics: Condensed Matter*, 5(5):559, 1993.

[30] Wen Wu, SH Brongersma, Marleen Van Hove, and Karen Maex. Influence of surface and grain-boundary scattering on the resistivity of copper in reduced dimensions. *Applied physics letters*, 84(15):2838–2840, 2004.

[31] QG Zhang, X Zhang, BY Cao, M Fujii, K Takahashi, and T Ikuta. Influence of grain boundary scattering on the electrical properties of platinum nanofilms. *Applied physics letters*, 89(11):114102, 2006.

[32] Tik Sun, Bo Yao, Andrew P Warren, Katayun Barmak, Michael F Toney, Robert E Peale, and Kevin R Coffey. Surface and grain-boundary scattering in nanometric cu films. *Physical Review B*, 81(15):155454, 2010.

[33] JR Sambles. The resistivity of thin metal filmssome critical remarks. *Thin Solid Films*, 106(4):321–331, 1983.

[34] KL Chopra, LC Bobb, and MH Francombe. Electrical resistivity of thin single-crystal gold films. *Journal of Applied Physics*, 34(6):1699–1702, 1963.

[35] Yoshikatsu Namba. Resistivity and temperature coefficient of thin metal films with rough surface. *Japanese Journal of Applied Physics*, 9(11):1326, 1970.

[36] KC Elsom and JR Sambles. Macroscopic surface roughness and the resistivity of thin metal films. *Journal of Physics F: Metal Physics*, 11(3):647, 1981.

[37] E Barborini, G Corbelli, G Bertolini, P Repetto, M Leccardi, S Vinati, and P Milani. The influence of nanoscale morphology on the resistivity of cluster-assembled nanostructured metallic thin films. *New Journal of Physics*, 12(7):073001, 2010.

[38] J Vancea, Horst Hoffmann, and K Kastner. Mean free path and effective density of conduction electrons in polycrystalline metal films. *Thin Solid Films*, 121(3):201–216, 1984.

[39] U Jacob, J Vancea, and H Hoffmann. Surface-roughness contributions to the electrical resistivity of polycrystalline metal films. *Physical Review B*, 41(17):11852, 1990.

[40] GH Gilmer and P Bennema. Simulation of crystal growth with surface diffusion. *Journal of Applied Physics*, 43(4):1347–1360, 1972.

[41] DE Wolf and J Villain. Growth with surface diffusion. *EPL (Europhysics Letters)*, 13(5):389, 1990.

[42] S Müller-Pfeiffer, H Van Kranenburg, and JC Lodder. A two-dimensional monte carlo model for thin film growth by oblique evaporation: simulation of two-component systems for the example of co cr. *Thin Solid Films*, 213(1):143–153, 1992.

[43] Liguo Wang and Paulette Clancy. Kinetic monte carlo simulation of the growth of polycrystalline cu films. *Surface Science*, 473(1):25–38, 2001.

[44] Peter Vang Hendriksen, Søren Linderoth, and P-A Lindgård. Finite-size modifications of the magnetic properties of clusters. *Physical Review B*, 48(10):7259, 1993.

[45] Dajie Zhang, KJ Klabunde, CM Sorensen, and GC Hadjipanayis. Magnetization temperature dependence in iron nanoparticles. *Physical Review B*, 58(21):14167, 1998.

[46] MJ Bonder, EM Kirkpatrick, T Martin, S-J Kim, RD Rieke, and Diandra L Leslie-Pelecky. Grain size effects on the magnetic properties of chemically synthesized ni: Ni 3 c nanocomposites. *Journal of magnetism and magnetic materials*, 222(1):70–78, 2000.

[47] Satish Vitta. Nonlinear spin wave magnetization of solution synthesized ni nanoparticles. *Journal of applied physics*, 101(6):063901, 2007.

[48] M Zheng, L Menon, H Zeng, Y Liu, Supriyo Bandyopadhyay, Roger D Kirby, and DJ Sellmyer. Magnetic properties of ni nanowires in self-assembled arrays. *Physical Review B*, 62(18):12282, 2000.

[49] AJ Freeman and Ru-quian Wu. Electronic structure theory of surface, interface and thin-film magnetism. *Journal of magnetism and magnetic materials*, 100(1):497–514, 1991.

[50] Richard H Kodama, Ami E Berkowitz, EJ McNiff Jr, and S Foner. Surface spin disorder in nife 2 o 4 nanoparticles. *Physical Review Letters*, 77(2):394, 1996.

[51] L Del Bianco, A Hernando, M Multigner, C Prados, JC Sanchez-Lopez, A Fernandez, CF Conde, and A Conde. Evidence of spin disorder at the surface–core interface of oxygen passivated fe nanoparticles. *Journal of applied physics*, 84(4):2189–2192, 1998.

[52] C Vázquez-Vázquez, MA López-Quintela, MC Buján-Núñez, and J Rivas. Finite size and surface effects on the magnetic properties of cobalt ferrite nanoparticles. *Journal of Nanoparticle Research*, 13(4):1663–1676, 2011.

[53] Shang Yuan Ren and John D Dow. Spin-flip transition rate due to electron-magnon scattering in ferromagnetic thin films. *Physical Review B*, 61(10):6934, 2000.

[54] Daniel Gall. Electron mean free path in elemental metals. *Journal of Applied Physics*, 119(8):085101, 2016.

[55] MA Angadi. Some transport properties of transition metal films. *Journal of materials science*, 20(3):761–796, 1985.